Research Article

Journal of Environmental Nanotechnology

Development and Characterization of S-glass Fiber/Bi_2O_3-reinforced Epoxy Hybrid Composites for Enhanced Mechanical Performance and Gamma Radiation Shielding

Gnanasekaran Sasikumar[1], G. Senthilkumar[2], Viranshu Kumar[3], T. Anand[4], V. Vimala[5] and R. Girimurugan[6*]

[1]Department of Mechanical Engineering, GMRIT Deemed to be University, Rajam, AP, India
[2]Department of Mechanical Engineering, Bannari Amman Institute of Technology, Sathyamangalam, TN, India
[3]Department of Mechanical Engineering, Arka Jain University, Jamshedpur, JH, India
[4]Department of Artificial Intelligence and Data Science, Nandha College of Technology, Perundurai, TN, India
[5]Department of Robotics and Automation, Erode Sengunthar Engineering College, Perundurai, TN, India
[6]Department of Mechanical Engineering, Nandha College of Technology, Perundurai, TN, India
Received: 20.06.2026 Accepted: 22.07.2026 Published: 30.09.2026
*girinctmech@gmail.com

ABSTRACT

Conventional epoxy composites offer low weight and good processability but provide limited gamma-ray attenuation and mechanical resistance, while lead-based shields are heavy and toxic. This study develops a lead-free multifunctional composite by combining silane-treated S-glass fibres and chemically precipitated Bi_2O_3 nanoparticles within an epoxy matrix. The composites were fabricated using mechanical mixing, ultrasonication, vacuum degassing, ambient curing, and post-curing. Their chemical, morphological, thermal, mechanical, and gamma-shielding characteristics were evaluated using FTIR, SEM, TGA, DSC, impact and three-point bending tests, and a cobalt-60/NaI(Tl) attenuation setup. The optimized composites achieved an impact strength of 8.4 kJ/m² and a maximum flexural strength of 195 MPa, representing improvements of approximately 171% and 112%, respectively, over neat epoxy. The EP/SGF-20/Bi_2O_3-25 composite exhibited the lowest HVL of 5.4 cm, compared with 9.9 cm for neat epoxy, confirming improved gamma-ray attenuation. These improvements resulted from the combined effects of strong fibre reinforcement, high-density Bi_2O_3 nanoparticles, and enhanced interfacial bonding produced by silane treatment. The developed composites provide a lightweight, lead-free material with integrated structural, thermal, and radiation-shielding functions, offering potential for medical shielding components, nuclear facilities, aerospace structures, and radiation-protection systems.

Keywords: Bi_2O_3; Epoxy composites; S-glass fibres; Radiation shielding; Nanoparticles; Gamma radiation.

1. INTRODUCTION

The increasing demand for lightweight, high-performance, and multifunctional materials has encouraged the development of polymer composites for structural and radiation-protection applications. Epoxy resin is widely used because of its mechanical strength, chemical resistance, dimensional stability, corrosion resistance, and ease of processing. However, its brittle behaviour and limited interaction with high-energy photons restrict its application in radiation-prone environments. The incorporation of fibrous reinforcements and high-density inorganic fillers offers an effective strategy for simultaneously improving the structural and radiation-shielding performance of epoxy composites. Mineral- and inorganic filler-reinforced epoxy systems have demonstrated considerable potential for lightweight gamma- and neutron-radiation protection (Urooge *et al.* 2026).

High-density and high-atomic-number fillers improve photon attenuation through enhanced absorption and scattering. Among these materials, bismuth oxide (Bi_2O_3) is a promising lead-free shielding filler because of its high density, high atomic number, chemical stability, and lower toxicity compared with conventional lead-based materials. Shielding performance is commonly evaluated using the half-value layer (HVL), tenth-value layer (TVL), and mean free path (MFP). $BiFeO_3$-filled PMMA/PEO nanocomposites exhibited reduced half-value layer (HVL) and tenth-value layer (TVL) values with increasing nanoparticle concentration, indicating enhanced gamma-ray attenuation and improved radiation shielding efficiency (Abdel-Kader *et al.* 2026). Bi_2O_3 nanoparticle-reinforced waste tire/EPDM composites exhibited lower HVL and TVL values as filler loading increased, demonstrating the effectiveness of high atomic number bismuth oxide nanoparticles in improving radiation shielding efficiency

(Özdemir and Yıldırım, 2026). These parameters represent the material thickness required to reduce the incident radiation intensity to one-half, the thickness required to reduce it to one-tenth, and the average distance travelled by a photon between successive interactions, respectively. Previous studies have reported reductions in these parameters with increasing Bi-containing filler concentrations, confirming the effectiveness of Bi_2O_3 for radiation attenuation (Putra *et al.* 2025, Unagar *et al.* 2026). Nevertheless, shielding efficiency depends strongly on filler concentration, particle dispersion, composite density, matrix type, and photon energy.

Different lead-free shielding systems have incorporated Bi_2O_3, Bi–Sn coatings, $CaCO_3$, graphene, and boron-containing fillers. Bi_2O_3-containing mortars and Bi–Sn-coated fibre composites have demonstrated improved attenuation of ionizing radiation (Al-Saleh *et al.* 2024; Dhand *et al.* 2024). Coral-derived $CaCO_3$ reinforced epoxy composites exhibited enhanced radiation shielding performance with 39.63% attenuation at 60 kVp (Tochaikul *et al.* 2025). Epoxy/hBN and graphene-based three-dimensional nanocomposites exhibited enhanced multifunctional performance with thermal conductivity compared to neat epoxy (Benedetti *et al.* 2025). However, many previous investigations primarily focused on radiation attenuation without sufficiently examining the relationship among shielding efficiency, mechanical integrity, thermal stability, and interfacial behaviour. Moreover, excessive particle loading may increase resin viscosity and cause agglomeration, void formation, and stress concentration. A hybrid reinforcement strategy is therefore required to improve radiation attenuation without compromising structural performance (Mengge *et al.* 2023).

S-glass fibres are suitable structural reinforcements because of their high strength, stiffness, impact resistance, thermal stability, and relatively low density. Previous investigations have demonstrated that S-glass reinforcement improves load-bearing capacity, flexural behaviour, impact resistance, and fracture toughness through efficient stress transfer, fibre bridging, fibre pull-out, and crack-deflection mechanisms (Mastan *et al.* 2022; Dalfi *et al.* 2022). Hybrid Palm fiber/S-glass composites (Venkatesan *et al.* 2021) and Coconut fiber/S-glass (Chandel *et al.* 2025) have further shown that strong fibre–matrix adhesion is essential for improving mechanical performance and fracture resistance. Nevertheless, S-glass fibres alone provide limited gamma-ray attenuation, whereas Bi_2O_3 nanoparticles enhance photon interaction but cannot independently provide effective crack bridging and structural reinforcement. Their combined use is therefore expected to provide complementary functions: S-glass fibres improve structural integrity, while Bi_2O_3 nanoparticles enhance gamma-ray absorption and scattering.

In polymer–metal oxide nanocomposites, appropriate binder and matrix selection is important for achieving nanoparticle compatibility, improved adhesive behaviour, and dispersion stability (Karthikeyan *et al.* 2024). The performance of this hybrid system strongly depends on the interface between the epoxy matrix and the reinforcing phases. Differences in surface chemistry may result in inadequate wetting, weak interfacial adhesion, fibre pull-out, and nanoparticle agglomeration. Silane treatment was therefore employed to introduce functional groups onto the surfaces of the S-glass fibres and Bi_2O_3 nanoparticles. These groups can interact with the inorganic reinforcement surfaces and the organic epoxy network, thereby improving wettability, particle dispersion, interfacial bonding, and stress transfer. Previous studies on silane-modified epoxy composites have demonstrated that surface treatment can improve filler dispersion, interfacial adhesion, mechanical strength, and durability (Somasundaram *et al.* 2024).

Existing Bi_2O_3/epoxy studies have mainly examined the relationship between particle concentration and radiation-attenuation parameters, whereas S-glass/epoxy investigations have generally focused on mechanical and fracture performance. Limited information is available on hybrid epoxy composites that combine silane-treated S-glass fibres with chemically synthesized Bi_2O_3 nanoparticles and systematically correlate their interfacial morphology with mechanical, thermal, and cobalt-60 gamma-ray attenuation performance. In particular, the effects of fibre and nanoparticle loading on the balance between structural reinforcement and shielding efficiency have not been adequately established. This constitutes the principal research gap addressed in the present study. The novelty of this work lies in developing a lead-free EP/SGF/Bi_2O_3 hybrid composite in which silane-treated S-glass fibres provide structural reinforcement and chemically precipitated Bi_2O_3 nanoparticles provide gamma-ray attenuation. Unlike conventional particulate Bi_2O_3/epoxy systems that are evaluated primarily for shielding performance, the present study investigates the combined chemical, morphological, mechanical, thermal, and radiation-attenuation behaviour of the hybrid composites. Furthermore, comparison with neat epoxy and S-glass/epoxy control specimens allows the individual and combined contributions of the fibrous and particulate reinforcements to be distinguished.

Accordingly, this study aims to: (i) synthesize Bi_2O_3 nanoparticles through a controlled chemical-precipitation method; (ii) apply silane treatment to S-glass fibres and Bi_2O_3 nanoparticles; (iii) fabricate epoxy composites containing different reinforcement concentrations; (iv) characterize their interfacial, morphological, mechanical, and thermal properties; and (v) evaluate their gamma-ray attenuation using a cobalt-60 source through linear attenuation coefficient, HVL, and TVL measurements. It is hypothesized that silane

treatment will improve reinforcement dispersion and interfacial adhesion and that the combined incorporation of S-glass fibres and Bi_2O_3 nanoparticles will produce better multifunctional performance than neat epoxy and fibre-only epoxy composites.

2. MATERIALS AND METHODOLOGY

2.1 Materials

Epoxy resin and its corresponding curing agent were procured from Kovai Cheenu Enterprises, Coimbatore, Tamil Nadu, India and used as matrix material without further purification. S-glass fibers were obtained from a certified composite reinforcement manufacturer (Go Green Enterprises, Chennai) and employed as the primary reinforcing phase. Chopped S-glass fibres with an average length of 6 ± 1 mm and diameter of approximately 10–15 µm were used. The fibres were randomly oriented within the epoxy matrix during mechanical mixing. [$Bi(NO_3)_3 \cdot 5H_2O$] Bismuth(III) nitrate pentahydrate, sodium hydroxide (NaOH), nitric acid (HNO_3), ethanol, and distilled water used for the synthesis of bismuth oxide (Bi_2O_3) nanoparticles were of analytical grade and purchased from Star Scientific Solutions, Erode, Tamil Nadu, India. The synthesized Bi_2O_3 nanoparticles served as the radiation-shielding filler in the composite system. Aminopropyl trimethoxysilane (GX-540) was used as the surface modification agent to improve the interfacial adhesion between the epoxy matrix, S-glass fibers, and Bi_2O_3 nanoparticles. All chemicals were used as received without any further purification.

2.2 Synthesis of Bismuth Oxide (Bi_2O_3)

Table 1. Hybrid composite formulations and their corresponding sample designations

Sample Designation	Formulation	EP (wt.%) (Epoxy Resin+Curing Agent)	SGF (wt.%)	Bi_2O_3 (wt.%)
S1	EP	100	-	-
S2	EP/SGF-10	90	10	-
S3	EP/SGF-10/ Bi_2O_3-15	75	10	15
S4	EP/SGF-10/ Bi_2O_3-25	65	10	25
S5	EP/SGF-20	80	20	-
S6	EP/SGF-20/ Bi_2O_3-15	65	20	15
S7	EP/SGF-20/ Bi_2O_3-25	55	20	25

Bismuth oxide (Bi_2O_3) was prepared through a precipitation-assisted synthesis route. Initially, 2.425 g of $Bi(NO_3)_3 \cdot 5H_2O$, bismuth(III) nitrate pentahydrate, corresponding to a 0.1 M concentration, was dissolved in 50 mL of deionized water. A small quantity of nitric acid was added to facilitate complete dissolution of the precursor salt. The solution was continuously stirred for 60 min to obtain a uniform precursor mixture. Subsequently, 1.0 M NaOH solution was added dropwise at approximately 1 mL·min^{-1} under continuous stirring at 600 rpm and 25 ± 2 °C until the pH reached 8.0 ± 0.1. The resulting suspension was stirred for an additional 30 min and aged for 2 h to complete precipitation before filtration and washing. Thereafter, the product was filtered and dried at 70 °C for 12 h in a hot-air oven. The dried precursor was subjected to calcination at 650 °C for 4 h in a furnace to induce phase transformation into Bi_2O_3 (Sarani *et al.* 2026). The calcined Bi_2O_3 was manually ground using an agate mortar and pestle for 30 min and passed through a 75 µm sieve. SEM analysis indicated an average particle size of approximately 45 ± 8 nm.

2.3 Preparation of Epoxy Resin Matrix

The epoxy resin matrix was prepared using a conventional resin-curing process. Initially, the required amount of epoxy resin was placed in a clean beaker and stirred mechanically at room temperature to obtain a uniform mixture. Subsequently, the curing agent (hardener) was added to the epoxy resin according to the manufacturer-recommended ratio of 10:1 (resin, by weight) and mixed thoroughly for 15 min until a homogeneous solution was obtained. The resulting mixture was then degassed under vacuum to remove entrapped air bubbles and ensure proper resin flow during composite fabrication. After degassing, the prepared epoxy composite was immediately used as the matrix material for the incorporation of silane-treated S-glass fibers and Bi_2O_3 filler particles. The final resin system obtained was designated as epoxy resin (EP) at following subsections.

2.4 Preparation of Hybrid Composites

Prior to composite fabrication, both the S-glass fibers (SGF) and synthesized Bi_2O_3 nanoparticles were subjected to silane surface treatment to improve their compatibility with the epoxy matrix. Initially, the reinforcing materials were dried in a vacuum oven at 80°C for 2 h to eliminate residual moisture. A 60:40 (v/v) ethanol–distilled water solution containing 0.9 g of aminopropyl trimethoxysilane was adjusted to pH 4.5 ± 0.1 using acetic acid and stirred at 500 rpm for 30 min at 25 ± 2 °C to promote silane hydrolysis. The dried S-glass fibres and Bi_2O_3 nanoparticles were then introduced, mechanically stirred for 5 h, and ultrasonicated for 30 min. The treated reinforcements were filtered, washed with ethanol, dried at 80 °C for 12 h, and cured at 110 °C for 2 h.

The hybrid composites were fabricated using the hand lay-up method. Silane-treated S-glass fibres and Bi_2O_3 nanoparticles were gradually incorporated into the epoxy–hardener mixture and mechanically stirred at 600

rpm for 20 min. The mixture was vacuum-degassed for 15 min, poured into release-agent-coated moulds, and manually levelled to obtain uniform specimens. The composites were cured at room temperature for 24 h and subsequently post-cured at 80 °C for 2 h.(Mohammed *et al.* 2026).

2.5 Characterization Procedures

Surface morphology and dispersion characteristics of S-glass fibers, Bi_2O_3 nanoparticles, and fractured composite samples were examined by scanning electron microscopy (ZEISS Gemini) at an accelerating voltage of 10 kV. The SEM were employed to investigate interfacial bonding between reinforcement and matrix phases, particle distribution, and failure mechanisms of fabricated composites.

Thermal degradation behavior was evaluated by thermogravimetric analysis. Fourier transform infrared spectroscopy (FTIR) measurements were carried out using a PerkinElmer Spectrum 100 spectrometer (Waltham, MA, USA) within the wavenumber range of 4000–400 cm^{-1} to identify the characteristic functional groups and investigate possible chemical interactions among the epoxy matrix, S-glass fibers, and Bi_2O_3 nanoparticles at a resolution of 4 cm^{-1} using 32 scans.

The flexural properties of composites were determined by an Instron 5569 universal testing machine. Three-point bending tests were conducted in accordance with ASTM D790-17 on specimens having dimensions of 127 × 12.7 × 3 mm^3 at a crosshead speed of 2 mm min^{-1}. Impact resistance was evaluated using a Tinius-Olsen impact testing machine according to ASTM D256-10. Notched specimens with 63.5 × 12.7 × 3 mm^3 were used for impact testing. Five specimens (n = 5) from each composite formulation were tested independently for both flexural and impact characterization. The results are reported as mean ± standard deviation.

Differential scanning calorimetry was performed using a TA Instruments Q200 calorimeter. The specimen was heated from 20°C to 350°C at a heating rate of 20°C min^{-1} under continuous nitrogen flow to evaluate the thermal transitions and curing behavior of the composites. TGA was conducted using approximately 10 mg of sample from 30 to 800 °C at a heating rate of 10 °C·min^{-1} under nitrogen flowing at 50 mL·min^{-1}.

Gamma-radiation shielding performance was investigated to assess the attenuation capability of the developed epoxy/S-glass fiber/Bi_2O_3 hybrid composites. The shielding experiments were conducted using NaI(Tl) scintillation detector with an active area of 300 mm × 300 mm for photon detection. A cobalt-60 source emitting gamma photons of 1.17 MeV was employed as the radiation source with an energy resolution of 4.9%. A ^60Co source with an activity of 10 µCi was positioned 30 cm from the detector. Composite thicknesses of 2, 4, 6, and 8 cm were tested for 300 s each, with three replicate measurements and background-count correction. To obtain a well-collimated radiation beam, a narrow aperture was introduced into the lead shielding enclosure surrounding the source. The transmitted photon intensity was recorded and subsequently used to analyse radiation attenuation characteristics of prepared composites.

Gamma radiation shielding test depicted in Fig. 1 were conducted at ambient temperature to determine the efficacy of fabricated materials in attenuating incident radiation.

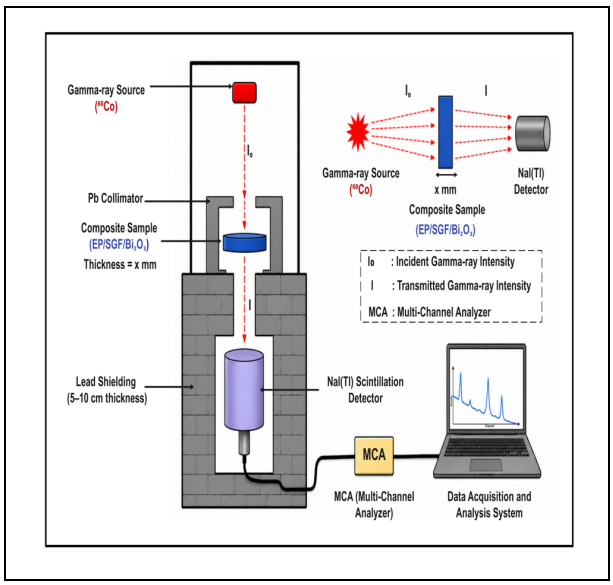

Fig. 1: Schematic view of experimental gamma-ray shielding setup

The Heat Resistance Index (THRI) equation (Yuvaraj *et al.* 2026):

$$T_{\mathrm{HRI}} = 0.49[T_5 + 0.6(T_{30} - T_5)] \quad \ldots (1)$$

where T_{HRI} is the heat resistance index, while T_5 and T_{30} represent the temperatures corresponding to 5% and 30% mass losses, respectively.

The radiation attenuation parameters were determined from the experimental measurements using the following equations:

The reduction in gamma-ray intensity through the shielding material was evaluated using Beer–Lambert attenuation principle (Krauklis *et al.* 2018).

$$I/I_0 = e^{-\mu x} \mathrm{or} \ln(I/I_0) = -\mu_L x \quad \ldots (2)$$

where I_0 represents incident photon intensity prior to interaction with the shielding medium, μ_L

corresponds to the linear attenuation coefficient of the shielding material and I denotes the transmitted photon intensity after passing through material of thickness x.

Half-value layer (HVL) and Tenth-value layer (TVL) were calculated using Eqs. (3) and (4).

$$HVL = X_h = \frac{\text{Ln}2}{\mu} \quad \ldots (3)$$

$$TVL = X_t = \frac{Ln10}{\mu} \quad \ldots (4)$$

3. RESULTS AND DISCUSSION

3.1 Surface Analysis of Reinforcing Phases

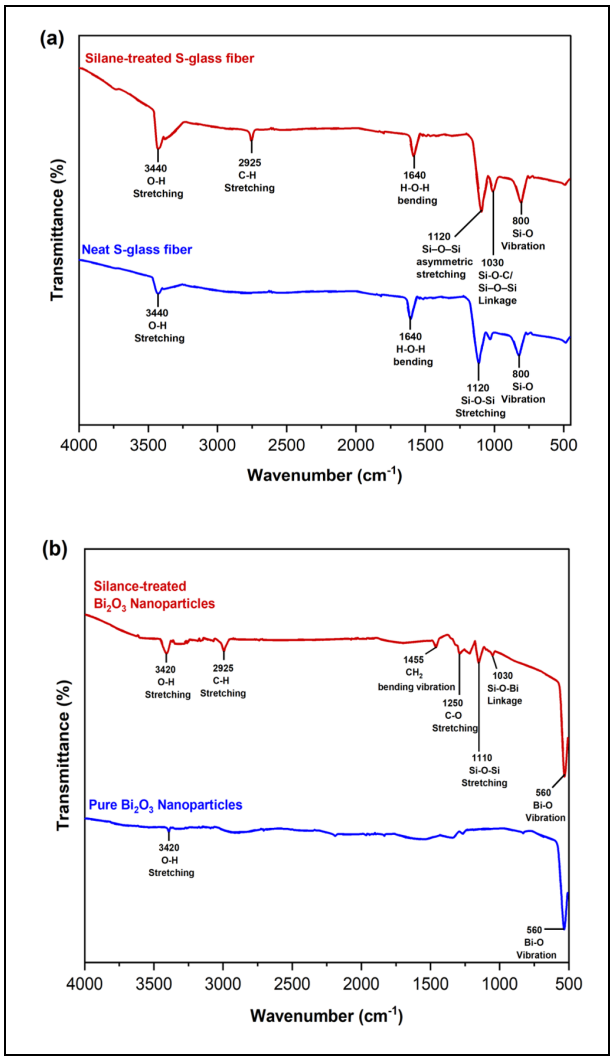

Fig. 2: (a) FTIR spectra of neat and silane-treated S-glass fibers (SGF) and (b) FTIR spectra of pure and silane-treated Bi_2O_3 nanoparticles

The improved performance of the hybrid composites resulted from changes in stress-transfer and crack-propagation mechanisms rather than merely from increasing reinforcement content. S-glass fibres carried the applied load and bridged developing cracks, whereas rigid Bi_2O_3 nanoparticles restricted localized polymer-chain deformation and promoted crack deflection. Silane treatment improved reinforcement wettability and reduced interfacial discontinuities, enabling more efficient stress transfer from the epoxy matrix to the reinforcing phases.

Silane treatment of S-glass fibers (SGF) and Bi_2O_3 nanoparticles enhanced their interfacial compatibility and dispersion within the epoxy (EP) matrix. The modification process introduced functional groups onto the SGF and Bi_2O_3 surfaces. The FTIR spectra obtained for the treated reinforcements are presented in Fig. 2.

The FTIR spectrum of untreated S-glass fibers exhibited characteristic absorption bands associated with silicate groups. A band near 800 cm^{-1} were attributed to Si–O vibration, while the prominent peak at 1120 cm^{-1} corresponded to Si–O–Si stretching vibrations. The untreated Bi_2O_3 nanoparticles displayed a prominent absorption peak around 560 cm^{-1} corresponding to Bi–O vibrations. The broad band observed at approximately 3440 cm^{-1} and the peak near 1640 cm^{-1} were associated with surface hydroxyl groups and adsorbed moisture. Following silane treatment, additional absorption bands appeared at 2925 cm^{-1} due to C–H stretching vibrations. Characteristic epoxy-related bands were detected at 1455 cm^{-1} and 1250 cm^{-1}, to C–H bending and C–O stretching vibrations. Furthermore, absorption bands at 1110–1120 cm^{-1} and 1030 cm^{-1} confirmed the formation of Si–O–Si and Si–O–C/Si–O–Bi linkages, indicating successful chemical interaction between the silane coupling agent and SGF/Bi_2O_3 surfaces. These observations verify the effectiveness of the surface modification treatment.

The proposed interfacial improvement is supported collectively by the FTIR bands associated with silane functional groups, the reduced interfacial gaps and fibre pull-out observed by SEM, and the corresponding improvements in impact and flexural properties. However, these results provide indirect rather than quantitative evidence of interfacial bonding; therefore, the term 'improved interfacial interaction' is used instead of claiming complete chemical bonding.

3.2 Structural Studies

FTIR analysis was employed to analyse the chemical interactions among the epoxy matrix, S-glass fibers, and Bi_2O_3 nanoparticles. As shown in Fig. 3, the characteristic epoxy absorption band near 915 cm^{-1} exhibited reduced intensity after curing, indicating the consumption of epoxy groups during crosslinking. The absorption bands around 2925 cm^{-1} corresponded to C–H stretching vibrations of the epoxy matrix. A broad band observed near 3440 cm^{-1} was attributed to hydroxyl groups formed during the curing process. Furthermore,

peaks detected at approximately 1105 cm^{-1} and 1600 cm^{-1} were associated with Si–O–Si asymmetric stretching vibrations of S-glass fibers and aromatic C=C vibrations of the epoxy structure, respectively. Additional absorption bands at 1508 cm^{-1}, 1245 cm^{-1}, and 1030 cm^{-1} corresponded to aromatic ring vibrations, C–O–C (epoxy) stretching, and Si–O–C/Si–O–Bi linkages, respectively, confirming the successful incorporation of silane-treated reinforcements into the epoxy matrix. The appearance of the 560 cm^{-1} absorption band further verified the presence of Bi–O vibrations associated with Bi_2O_3 nanoparticles. These results confirm effective interfacial interaction between the epoxy matrix, S-glass fibers, and Bi_2O_3 nanoparticles. Following silane treatment, changes in the broad O–H region and the appearance or strengthening of bands associated with amino-organosilane groups indicated silane adsorption and condensation on the reinforcement surfaces. Nevertheless, FTIR alone cannot conclusively establish covalent bonding; therefore, these spectral changes were interpreted as evidence of surface modification and possible interfacial interaction. In previous studies, FTIR characterization demonstrated the presence of surface functional groups capable of improving interfacial bonding between natural fibers and polymer matrices, thereby contributing to enhanced composite performance (Loganathan *et al.* 2025).

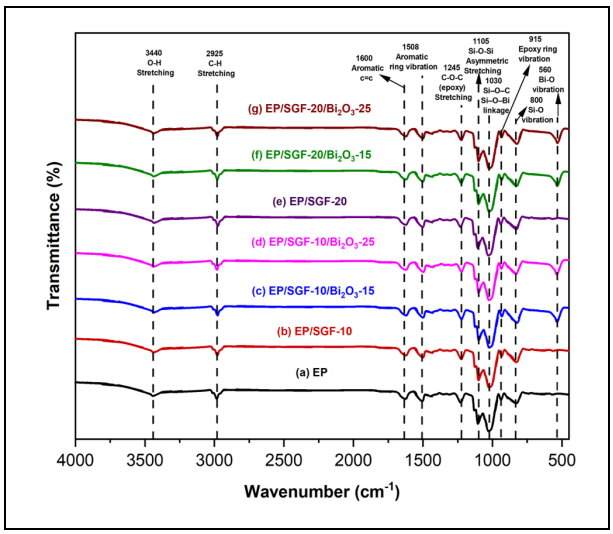

Fig. 3: FTIR spectra of EP, EP/SGF, and EP/SGF/Bi_2O_3 hybrid composites

3.3 TGA Analysis

TGA test was performed to analyze the behavior of both fabricated polymer composites and pure polymers under high-temperature conditions, as seen in Fig. 4.

Furthermore, the authors gathered critical thermal metrics, including the starting thermal breakdown temperatures, the temperature corresponding to char yields at 800°C, and the heat resistance index.

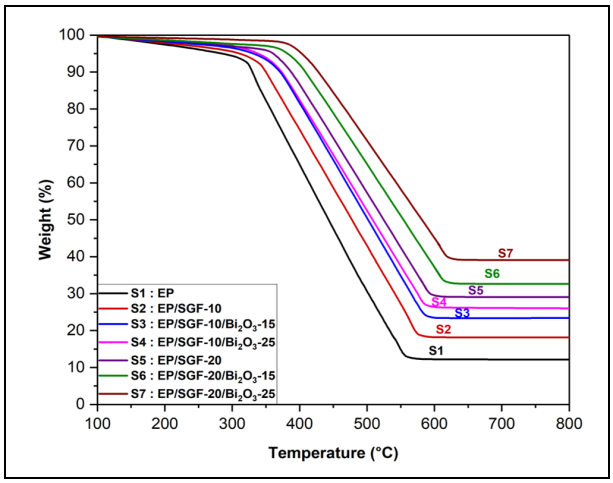

Fig. 4: Thermogravimetric analysis (TGA) of EP/SGF/Bi_2O_3 hybrid composites

Table 2. Thermal property parameters of hybrid composites with varying fibers and particles

Sample	Formulation	$T_{5wt\%}$(°C)	$T_{10wt\%}$ (°C)	$T_{30wt\%}$(°C)	T_{HRI}(°C)	Y_c (%)
S1	EP	320.5	345.8	425.3	185.4	12.1
S2	EP/SGF-10	338.4	368.2	472.6	201.8	18.0
S3	EP/SGF-10/ Bi_2O_3 − 15	347.6	381.5	495.4	214.3	23.2
S4	EP/SGF-10/ Bi_2O_3 − 25	356.2	392.8	518.7	226.9	26.0
S5	EP/SGF-20	362.5	399.4	525.6	233.8	29.1
S6	EP/SGF-20/ Bi_2O_3 − 15	371.4	411.2	548.3	245.7	33.0
S7	EP/SGF-20/ Bi_2O_3 − 25	385.8	425.6	575.9	261.4	39.0

Initially, the neat epoxy (EP) resin exhibited the lowest thermal stability among all fabricated specimens. The T_5wt%, T_{10}wt%, THRI, and Yc values were determined as 320.5°C, 345.8°C, 185.4°C, and 12.1%, respectively. As illustrated in Fig. 4, the addition of S-glass fibers (SGF) improved the thermal resistance of the epoxy matrix. For the EP/SGF (20 wt.%) composite, T_5wt%, T_{10}wt%, THRI, and Yc values increased to 362.5°C, 399.4°C, 233.8°C, and 29.1%, respectively. This improvement was attributed to the ability of SGF to retard thermal degradation and restrict the mobility of epoxy molecular chains. Furthermore, hybrid incorporation of Bi_2O_3 nanoparticles along with SGF resulted in additional enhancement of the thermal degradation parameters. Compared with SGF-reinforced composites, the hybrid composites exhibited noticeable increases in T_5wt%, T_{10}wt%, THRI, and Yc, demonstrating the beneficial effect of combining fiber and nanoparticle reinforcements. The EP/SGF-20/Bi_2O_3-25 composite exhibited the highest thermal stability with T_5wt%, T_{10}wt%, THRI, and Yc values of 385.8°C, 425.6°C, 261.4°C, and 39.0%, respectively. Superior thermal behavior of hybrid composites is associated with the excellent thermal stability of both SGF and Bi_2O_3 particles. As shown in Fig. 5, the reinforcing phases maintained their structural integrity throughout the investigated temperature range, with S-glass fibers and Bi_2O_3 nanoparticles retaining approximately 97.2% and 99.1% of their initial weight at 800°C, respectively. The higher residual weight of Bi_2O_3 confirms its outstanding thermal resistance and its ability to act as an effective thermal barrier within the epoxy matrix. The synergistic interaction between the reinforcing constituents effectively delayed the decomposition of the epoxy matrix. In addition, strong interfacial adhesion and uniform dispersion among the epoxy resin, SGF, and Bi_2O_3 nanoparticles contributed to the enhanced thermal performance of the developed hybrid composites.

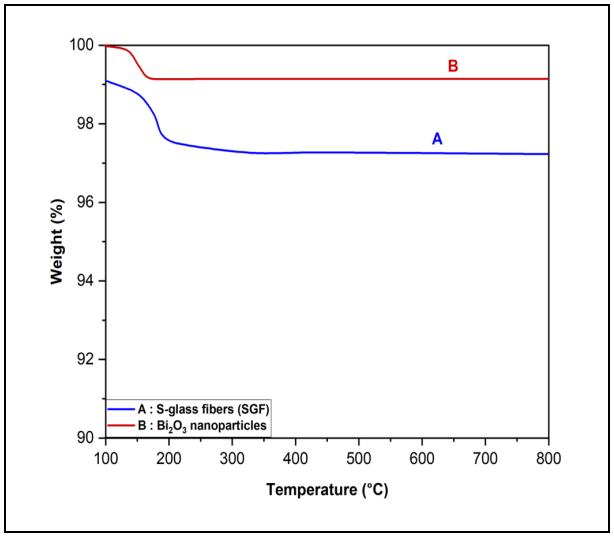

Fig. 5: Thermal stability of S-glass fibers (SGF) and Bi_2O_3 nanoparticles obtained from thermogravimetric analysis

The TGA curves indicated multiple degradation stages, including initial removal of absorbed moisture and low-molecular-weight species, followed by decomposition of the crosslinked epoxy network and subsequent carbonaceous-residue formation. A separate derivative thermogravimetric analysis was not performed; therefore, the precise maximum degradation temperatures and overlapping decomposition stages could not be resolved. DTG analysis is recommended in future work to identify the individual degradation peaks more accurately.

3.4 Impact Strength Analysis

To evaluate the influence of varying S-glass fiber (SGF) and Bi_2O_3 nanoparticle loadings on the impact resistance of fabricated composites, impact testing was conducted, and the results were presented in Fig. 6.

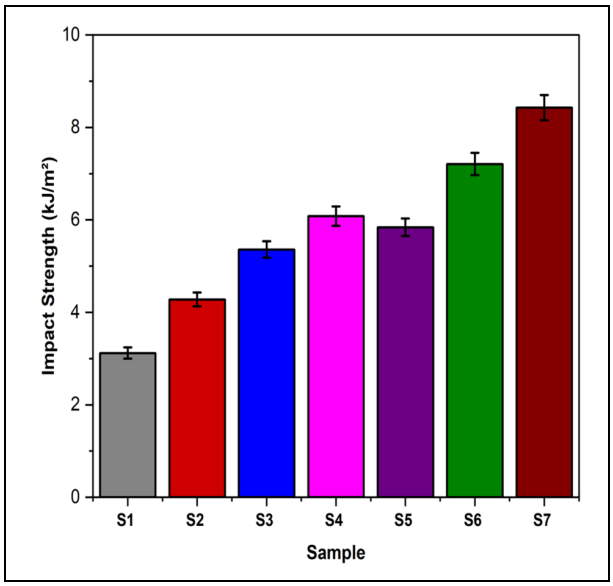

Fig. 6: Impact strength behavior of the EP/SGF/Bi_2O_3 hybrid composites

Initially, the neat epoxy (EP) resin exhibited the lowest impact strength among all tested specimens, recording approximately 3.1 kJ/m. The behavior was attributed to the inherent brittleness of the crosslinked epoxy matrix, which offers limited resistance to sudden impact loading. Under applied impact forces, localized stress concentrations can initiate microcracks that subsequently propagate through the matrix, leading to premature failure. The incorporation of S-glass fibers (SGF) progressively enhanced the impact performance of composites. The highest IS of approximately 8.4 kJ/m² was obtained for the EP/SGF-20/Bi_2O_3-25 hybrid composite, corresponding to an improvement of about 171% compared with neat epoxy. Enhanced impact resistance was attributed to the high strength of SGF, the reinforcing effect of Bi_2O_3 nanoparticles, and the strong interfacial adhesion achieved through silane treatment.

Furthermore, the uniform dispersion of reinforcing phases within the epoxy matrix facilitated stress transfer and improved the ability of composites to withstand impact loading. According to previous studies, the optimized TFS3 hybrid composite achieved an impact energy of 4.9 J and absorbed 39 J under low-velocity impact loading, indicating enhanced impact tolerance due to effective interfacial bonding and uniform filler dispersion (Kumar *et al.* 2026a).

3.5 Three-point Bending Test

Flexural strength and modulus of epoxy-based hybrid reinforced with loadings of S-glass fibers (SGF) and Bi_2O_3 nanoparticles were determined using a three-point bending test, and the obtained outcomes were illustrated in Fig. 7.

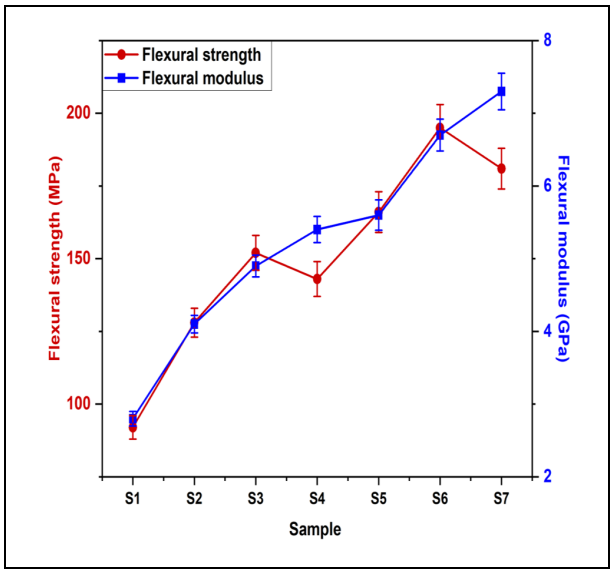

Fig. 7: Flexural strength and flexural modulus of EP/SGF/Bi_2O_3 hybrid composites

As illustrated in Fig. 7, the neat epoxy (EP) resin exhibited the lowest flexural properties among all tested specimens, with a flexural strength of approximately 92 MPa and a flexural modulus of 2.8 GPa. This behavior was attributed to the relatively brittle nature of the crosslinked epoxy network, which limits its ability to withstand high bending loads and makes it more susceptible to crack propagation and initiation under flexural stress. As a result, the neat epoxy matrix demonstrates limited resistance to deformation subjected to bending forces. Incorporation of S-glass fibers (SGF) and Bi_2O_3 nanoparticles markedly improved both flexural strength and modulus, indicating the effectiveness of these reinforcements in improving the mechanical performance of the epoxy matrix. The highest flexural strength of approximately 195 MPa was observed for EP/SGF-20/Bi_2O_3-15 (S6), while the maximum flexural modulus of approximately 7.4 GPa was achieved by EP/SGF-20/Bi_2O_3-25 (S7), corresponding to improvements of approximately 112% in FS and 164% in flexural modulus compared with neat epoxy. These significant increases demonstrate a synergistic effect of combining particulate and fibrous reinforcements within the polymer matrix. The enhancement in flexural performance was attributed to the high stiffness and strength of SGF, the reinforcing effect of Bi_2O_3 nanoparticles, and the efficient transfer of applied stress across the matrix–reinforcement interface. In addition, the presence of rigid nanoparticles helps restrict polymer chain mobility, thereby improving the resistance of the composite to bending deformation. Furthermore, silane treatment promoted stronger interfacial bonding between the epoxy matrix and reinforcing phases, reducing the likelihood of interfacial debonding under loading. The uniform dispersion of the reinforcing phases also contributed to improved load-bearing capability, better stress distribution throughout the composite structure, and enhanced fracture resistance. Consequently, the hybrid composites showed higher flexural behavior compared with the neat epoxy resin, highlighting their potential for applications requiring high stiffness, strength, and durability under bending loads. In previous studies, Hybrid glass/flax fibre-reinforced PP/PB composites exhibited a 15% improvement in flexural strength, demonstrating the effectiveness of hybrid fibre reinforcement in enhancing load-bearing capability and structural performance (Diwahar *et al.* 2024).

The non-linear response to reinforcement loading indicates that composite performance was governed by the balance between reinforcement efficiency and defect formation. At suitable concentrations, the fibres and nanoparticles improved load transfer and restricted crack growth. At higher local concentrations, particle–particle interaction and increased mixture viscosity could reduce nanoparticle distribution and create stress-concentration regions, limiting further improvement. The maximum flexural strength obtained in this study was 195 MPa for S6, exceeding the 162 MPa reported for a silane-treated hybrid epoxy composite (Jayanthi *et al.* 2024) and the 160 MPa reported for a silane-treated microfibre/lignin epoxy system (Kumar *et al.* 2026b). The higher value obtained here suggests that the combined S-glass/Bi_2O_3 reinforcement and silane-assisted interface provided effective resistance to bending-induced crack propagation. However, differences in reinforcement type, specimen geometry, and testing conditions should be considered when interpreting this comparison.

Among the investigated formulations, S7 provided the best overall multifunctional performance. Its 20 wt.% S-glass content promoted fiber bridging and load transfer. Consequently, S7 achieved the highest impact strength of 8.4 $kJ \cdot m^{-2}$, maximum flexural modulus of 7.4 GPa, and char yield of approximately 39%. Although S6 exhibited the highest flexural strength of 195 MPa, S7 offered the most favorable overall

balance of impact resistance, stiffness and thermal stability.

3.6 Nuclear Shielding Investigations

The gamma-radiation shielding capability of the developed epoxy/S-glass fiber/Bi_2O_3 hybrid composites was systematically evaluated to determine their suitability for radiation protection applications. Particular attention was given to assessing their potential as lightweight alternatives to shielding materials used at nuclear, industrial, and medical environments. The linear attenuation coefficient (μL), presented in Fig. 8, was selected as a key parameter for quantifying the interaction of gamma photons with the composite structure. Higher μL values indicate greater attenuation efficiency and improved shielding performance. The obtained outcomes show that the incorporation of S-glass fibers and Bi_2O_3 nanoparticles significantly improved the ability of the epoxy matrix to absorb and attenuate incident gamma radiation. Owing to the atomic number and high density of Bi_2O_3, hybrid composites exhibited improved photon attenuation characteristics, thereby reducing the transmission of gamma-ray energy through the material. Consequently, the developed composites show considerable promise for use in advanced radiation-shielding systems where reduced weight, structural integrity, and effective attenuation performance are required. According to previous studies, Monte Carlo simulations revealed that boron-containing epoxy resin offers enhanced neutron–gamma shielding performance, highlighting the potential of epoxy-based composites for structural and functional nuclear shielding applications (Xiao *et al.* 2023).

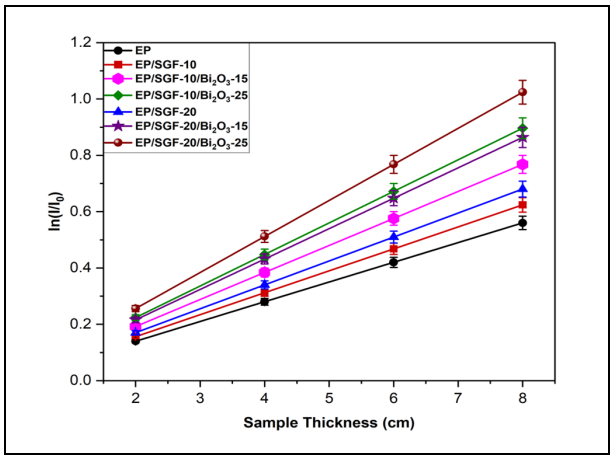

Fig. 8: Variation of $\ln(I_0/I)$ with sample thickness for EP/SGF/Bi_2O_3 composites at different reinforcement loadings

As illustrated in Fig. 8, the neat epoxy (EP) specimen exhibited the lowest linear attenuation behavior, with $\ln(I_0/I)$ increasing from approximately 0.14 at 2 cm to 0.56 at 8 cm. The incorporation of S-glass fibers and Bi_2O_3 nanoparticles improved the attenuation capability of composites. Among all formulations, EP/SGF-20/Bi_2O_3-25 exhibited the highest attenuation performance, with $\ln(I_0/I)$ values increasing from approximately 0.25 at 2 cm to 1.02 at 8 cm. The improved shielding performance is primarily attributed to the high density and high atomic number of Bi_2O_3 nanoparticles, which improve photon absorption and scattering within the composite structure.

To further evaluate the shielding effectiveness of the developed materials, tenth-value layer and half-value layer parameters were determined, and the corresponding results are presented in Fig. 9. The neat epoxy sample exhibited the highest HVL and TVL values of approximately 9.9 cm and 32.9 cm, respectively, indicating the lowest shielding efficiency. The incorporation of 20 wt.% S-glass fibers reduced HVL and TVL values to approximately 8.2 cm and 27.1 cm. Further addition of Bi_2O_3 nanoparticles significantly enhanced the attenuation capability, reducing the HVL and TVL values to 6.4 cm and 21.3 cm for EP/SGF-20/Bi_2O_3-15 and to 5.4 cm and 18.0 cm for EP/SGF-20/Bi_2O_3-25. The progressive reduction in HVL and TVL demonstrates the effectiveness of the hybrid reinforcement system in improving gamma-ray attenuation performance. Consequently, the EP/SGF-20/Bi_2O_3-25 composite exhibited the best radiation shielding capability among all fabricated specimens. Previous studies reported HVL values of 0.78–3.07 cm and TVL values of 2.58–10.19 cm for Bi_2O_3-GO/epoxy composites, confirming the effectiveness of Bi_2O_3-based epoxy systems in reducing photon penetration and enhancing gamma-ray shielding performance (Khalil *et al.* 2024).

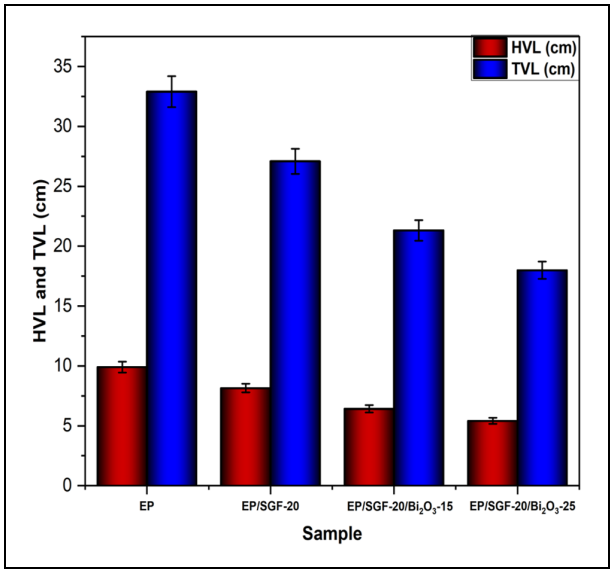

Fig. 9: Half-value layer (HVL) and tenth-value layer (TVL) of selected EP/SGF/Bi_2O_3 composites

The tenth-value layer and half-value layer show the thickness of shielding material needed to lower

incident gamma-ray intensity to one-half and one-tenth of its original value. These parameters are widely recognized as important indicators of the effectiveness of radiation-shielding materials. In the present investigation, HVL and TVL were determined for epoxy-based hybrid composites with S-glass fibers (SGF) and Bi_2O_3 nanoparticles. As illustrated in Fig. 9, hybrid composites exhibited lower HVL and TVL values than the neat epoxy matrix, indicating superior gamma-radiation attenuation capability. The neat epoxy specimen recorded the highest HVL and TVL values of approximately 9.9 cm and 32.9 cm, respectively, owing to its limited photon interaction capability. In contrast, the EP/SGF-20/Bi_2O_3-25 composite exhibited the lowest HVL and TVL values of approximately 5.4 cm and 18.0 cm, respectively, demonstrating the most effective shielding performance. The increase in radiation protection was attributed to the high density and high atomic number of Bi_2O_3, which significantly enhance photon absorption and scattering processes. In addition, the incorporation of SGF contributed to structural integrity and facilitated uniform distribution of shielding filler throughout the matrix. Consequently, the hybrid reinforcement system effectively reduced gamma-ray transmission and improved the overall attenuation performance of composites.

The S7 composite exhibited an approximate linear attenuation coefficient of 0.128 cm^{-1}, calculated from the slope of ln(I0/I) against thickness. This value was higher than the approximately 0.095–0.110 cm^{-1} reported for boron-rich slag/epoxy composites exposed to Co-60 radiation (Dong *et al.* 2023). Correspondingly, the S7 formulation achieved an HVL of approximately 5.4 cm, compared with 6.3–7.2 cm for the reported boron-rich slag systems. This comparison indicates improved high-energy attenuation, although differences in composition, density, geometry, and source conditions must be considered.

The outcomes demonstrate that epoxy/SGF/Bi_2O_3 hybrid composites exhibit competitive attenuation performance when compared with several polymer-based shielding systems reported in the literature. The enhanced shielding efficiency, combined with the advantages of low weight, corrosion resistance, ease of processing, and mechanical robustness, highlights the potential of these composites as alternative materials for radiation protection applications. Furthermore, unlike traditional metallic shielding materials, the developed hybrid composites offer improved design flexibility and reduced fabrication complexity while maintaining satisfactory gamma-ray attenuation characteristics. The shielding analysis was limited to the gamma photons emitted by the Co-60 source. Consequently, the present results primarily represent attenuation within the investigated high-energy region and should not be generalized to the entire photon-energy spectrum. Future studies should employ multiple sources, such as Am-241, Ba-133, Cs-137, and Co-60, together with Monte Carlo or XCOM calculations, to evaluate energy-dependent attenuation mechanisms.

3.7 Morphology Analysis

Following mechanical characterization, scanning electron microscopy (SEM) were employed to investigate the fracture morphology of fabricated EP/SGF/Bi_2O_3 composites, and the corresponding micrographs are presented in Fig. 10. The fracture surface of the neat epoxy matrix (fig. 10a) exhibited a relatively smooth morphology with distinct crack lines and cleavage-like features, indicating the brittle fracture behavior of the unreinforced thermoset resin. The presence of long crack paths suggests rapid crack propagation through the epoxy matrix with limited energy absorption during failure.

In contrast, the reinforced composites (fig. 10b and 10c) displayed significantly rougher fracture surfaces characterized by fiber pull-out, fiber fracture, matrix tearing, and irregular fracture features. In fig. 10b, embedded and fractured S-glass fibers can be clearly observed within the epoxy matrix, indicating effective load transfer among matrix and reinforcement. The presence of broken fibers rather than extensive fiber pull-out suggests improved interfacial adhesion resulting from the silane treatment. Furthermore, evidence of matrix deformation surrounding the fibers indicates that crack propagation was hindered by the reinforcing phases, thereby increasing the energy required for fracture.

Fig. 10c reveals a more compact and irregular fracture morphology with fewer continuous crack paths, indicating enhanced fracture resistance. The rough fracture surface and localized agglomerated regions suggest the presence of Bi_2O_3-rich domains embedded within the epoxy matrix. These regions act as obstacles to crack growth and contribute to crack pinning mechanisms and crack deflection during fracture. The combined action of S-glass fibers and Bi_2O_3 nanoparticles effectively restricted crack propagation, improved stress distribution within composite, and improved overall mechanical performance of hybrid composite.

Overall, the SEM observations confirm that, the incorporation of silane-treated S-glass fibers and Bi_2O_3 nanoparticles improved fracture resistance of the epoxy matrix through fiber bridging, fiber fracture, crack deflection, and particle-assisted crack arrest mechanisms, which are consistent with the improved impact and flexural properties observed for the developed hybrid composites. Similar observations have been reported in Bi_2O_3-based radiation shielding composites, where excessive filler loading promoted particle agglomeration, while optimized formulations maintained a more

homogeneous particle distribution and improved composite performance (Li *et al.* 2022). SEM observations indicated particle-containing regions within the epoxy matrix; however, SEM morphology alone cannot conclusively verify the spatial distribution of bismuth. Future work will incorporate EDS elemental mapping to further validate Bi distribution and quantitatively assess local particle accumulation within the epoxy matrix.

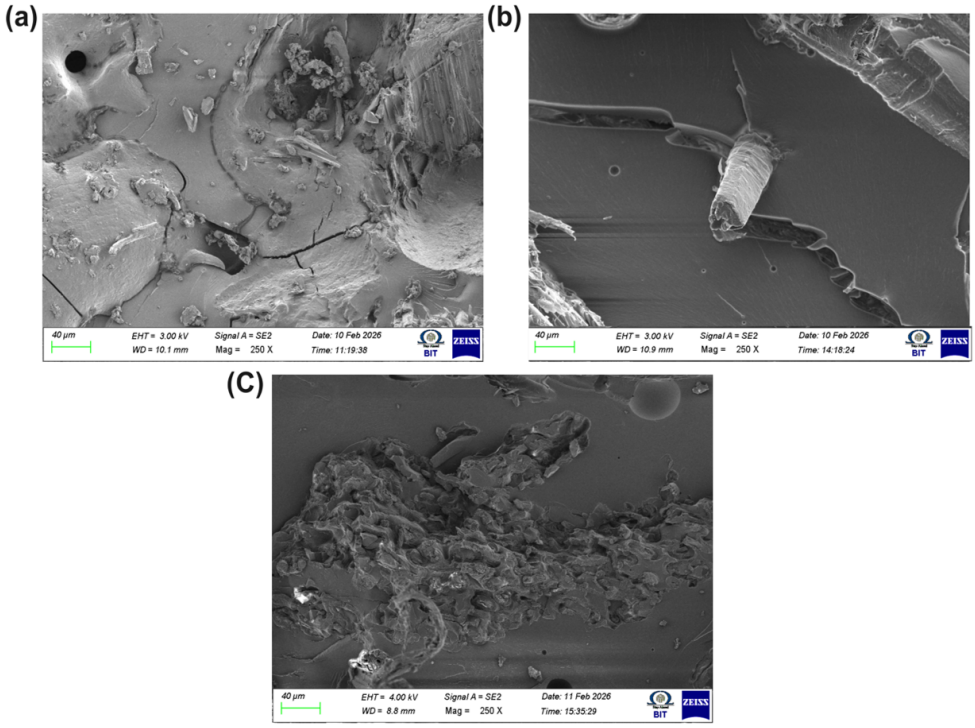

Fig. 10: SEM micrographs of the fracture surfaces of EP/SGF/Bi_2O_3 hybrid composites

4. CONCLUSIONS

This study developed a lead-free multifunctional epoxy composite by combining silane-treated S-glass fibres with chemically synthesized Bi_2O_3 nanoparticles. The scientific contribution lies in integrating the crack-bridging and load-transfer functions of S-glass fibres with the high-density photon-attenuation capability of Bi_2O_3 within a surface-modified epoxy system. The combined FTIR, SEM, thermal, mechanical, and shielding results indicate that improved matrix–reinforcement interaction enabled the composites to maintain structural integrity while accommodating a relatively high concentration of radiation-shielding filler. Among the investigated formulations, S7 containing 20 wt.% S-glass fibres and 25 wt.% Bi_2O_3 provided the best overall balance of impact resistance, stiffness, thermal stability, and gamma-ray attenuation, although S6 produced the highest flexural strength. The S7 composite achieved an approximate linear attenuation coefficient of 0.128 cm^{-1} and an HVL of 5.4 cm, compared with the reported values of 0.095–0.110 cm^{-1} and 6.3–7.2 cm for boron-rich slag/epoxy composites under Co-60 radiation. This comparison demonstrates competitive shielding performance while retaining the lightweight, corrosion-resistant, and processable characteristics of a polymer composite. The present shielding assessment was limited to Co-60 radiation and laboratory-scale specimens. In addition, DTG analysis and EDS elemental mapping were not included. Therefore, the suitability of the composite for medical, nuclear, or aerospace components requires application-specific validation involving realistic radiation fields, environmental exposure, long-term ageing, and structural loading. Future studies will incorporate multi-energy photon sources, Monte Carlo or XCOM simulations, DTG analysis, EDS mapping, irradiation durability testing, and pilot-scale fabrication. These investigations will further establish the energy-dependent shielding mechanisms, reinforcement distribution, long-term reliability, and practical applicability of the developed EP/SGF/Bi_2O_3 composites.

FUNDING

This research received no specific grant from any funding agency in the public, commercial, or not-for-profit sectors.

CONFLICTS OF INTEREST

The authors declare that there is no conflict of interest.

COPYRIGHT

This article is an open-access article distributed under the terms and conditions of the Creative Commons Attribution (CC BY) license (http://creativecommons.org/licenses/by/4.0/).

REFERENCES

Abdel-Kader, M. H., Mohamed, M. B., Khatab, A., Ibrahim, R. M. and El-Zohary, S. E., Multifunctional PMMA/PEO/$BiFeO_3$ nanocomposite films for enhanced optical, magnetic, and radiation shielding applications, *Radiat. Phys. Chem.*, 246, 113951 (2026). https://doi.org/10.1016/j.radphyschem.2026.113951

Al-Saleh, W. M., Elsafi, M., Almutairi, H. M., Nabil, I. M. and El-Nahal, M. A., A comprehensive study of the shielding ability from ionizing radiation of different mortars using iron filings and bismuth oxide, *Sci. Rep.*, 14(1), 10014 (2024). https://doi.org/10.1038/s41598-024-60188-2

Benedetti, L., Orikasa, K., Aleman, A., John, D. and Agarwal, A., Enhancing polymer composites: The impact of three-dimensional nanomaterial architectures on thermal, electrical, and radiation shielding properties, *Compos. Part A: Appl. Sci.,* 198, 109110 (2025). https://doi.org/10.1016/j.compositesa.2025.109110

Chandel, P. S., Somani, N., Gupta, N. K., Jain, A. and Elrashidi, A., Development and Characterization of Hybrid Coconut-S-Glass Fiber Composites for Enhanced Mechanical and Thermal Performance, *J. Compos. Sci.*, 9(9), 488 (2025). https://doi.org/10.3390/jcs9090488

Dalfi, H., Potluri, P., Jan, K. and Selver, E., Improving the fracture toughness of glass/epoxy laminates through intra-yarns hybridization, *Proce. Institut. Mech. Eng. Part L: J. Mater. Des. Appl.*, 236(9), 1750–1763 (2022). https://doi.org/10.1177/14644207221082224

Dhand, V., Hyunsuk, C., Hassan, T., Koo, C. M. and Rhee, K. Y., Tailored eutectic alloy coatings for enhanced EMI and X-ray protection by basalt fiber CNT/epoxy composite, *J. Mater. Res. Technol.*, 31, 689–697 (2024). https://doi.org/10.1016/j.jmrt.2024.06.096

Diwahar, P., Prakalathan, K., Bhuvana, K. P. and Senthilkumar, K., Examining the Mechanical and Thermal Properties of a Novel Hybrid Thermoplastic Rubber Composite Made with Polypropylene, Polybutadiene, S-Glass Fibre, and Flax Fibre, *Polym.*, 16(24), 3599 (2024). https://doi.org/10.3390/polym16243599

Dong, M., Zhou, S., Ge, C., Yang, H., Liu, M., Lakshminarayana, G. and Xue, X., Green and low-carbon upcycling of ludwigite: Prepared shields against nuclear radiation hazards and shielding mechanism, *Radiat. Phy. Chem.*, 208, 110931 (2023). https://doi.org/10.1016/j.radphyschem.2023.110931

Jayanthi, G., Andal, V., Prabaharan, M. and Geetha, P., Effect of silane-functionalized green synthesized silver nanoparticle, ferrite, and silk microfiber epoxy composite on electromagnetic interference shielding, *J. Mater. Sci. Mater. Electron.*, 35(34), 2158 (2024). https://doi.org/10.1007/s10854-024-13929-y

Karthikeyan, S., Manivannan, S., Venkatesh, R., Karthikeyan, S., Atanu, K. and Lakshmanan, S., Impact of Binder Selection on Functional Properties of Polymer Nanocomposite Featured with Metal Oxide Nanoparticle*, J. Environ. Nanotechnol*., 13(3), 262-270 (2024). https://doi.org/10.13074/jent.2024.09.242751

Khalil, W. F., Mubarak, F., Agha, A., Zaky, R. S. and Kamel, F. A., Investigation of the gamma ray shielding properties of Epoxy based on Bi_2O_3/GO nanocomposite, *J. Phys. Conf. Series*, 2830(1), 012023 (2024). https://doi.org/10.1088/1742-6596/2830/1/012023

Krauklis, A. E., Gagani, A. I. and Echtermeyer, A. T., Near-infrared spectroscopic method for monitoring water content in epoxy resins and fiber-reinforced composites, *Mater.*, 11(4), 586 (2018). https://doi.org/10.3390/ma11040586

Kumar, D. V., Mohanasundaram, S., Karthikeyan, S. K., Singh, A. K., Prasad, K. D. V., Nagabhooshanam, N., Balasubramanian, M., Kumar, N. S. and Sree, S. R., Load Bearing Properties of Sand Blasted SS304 Wire-Mesh and Silane-treated Pineapple/flax-Reinforced Si_2N_2O Modified Epoxy Resin Composites, *Waste Biomass Valoriz.*, 17(3), 1503–1517 (2026a). https://doi.org/10.1007/s12649-025-03198-z

Kumar, P. S., Soundararajan, R., Raffik, R. and Ali, L. F., Mechanical and functional performance of epoxy composites reinforced with cluster bean fibers and balloon vine stem lignin, *Polym. Bull.*, 83(4), 208 (2026b). https://doi.org/10.1007/s00289-025-06123-5

Li, W., Peng, M., Zhao, X. and Chen, S., Properties of Bi_2O_3/epoxy resin–coated composites for protection against gamma rays, *J. Indus. Tex.*, 51(5_suppl), 7545S-7568S (2022). https://doi.org/10.1177/15280837211051102

Mastan, V., Kishore Nath, N. and Deva Kumar, M. L. S., The Effect of Ath Addition on Mechanical Properties of Woven S-Glass/Epoxy Based Hybrid Composites, *J. Balkan Tribol. Associat.*, 28(3), 393–401 (2022). https://www.scopus.com/pages/publications/85135570342?origin=resultslist

Mengge, D., Zhou, S., Yang, H. and Xue, X., Gamma ray attenuation behaviors and mechanism of boron rich slag/epoxy resin shielding composites, *Nuclear Eng. Technol.,* 55(7), 2613–2620 (2023). https://doi.org/10.1016/j.net.2023.04.041

Mohammed, R., Shaik, A. S., Maneesha, L. L. S., Subrahmanyeswara Rao, S. V. B., Mohammed, S. and Murthy, K. K., Mechanical performance and python-based TOPSIS ranking of carbon-filled Kevlar/Basalt/S-glass hybrid epoxy composites for automotive structural applications, *Sci. Rep.*, 16(1), 12228 (2026). https://doi.org/10.1038/s41598-026-44376-w

Özdemir, T. and Yıldırım, I., Towards sustainability: Production and evaluation of waste tire and bismuth based radiation shielding material, *Radiat. Phy. Chem.*, 245, 113874 (2026). https://doi.org/10.1016/j.radphyschem.2026.113874

Putra, O. A., Saputra, D. N. I. and Arafat, F. B., A review of bismuth oxide (Bi_2O_3) based polymer composites: physical, structural, and gamma shielding properties, *Radiat. Effects Defects Sol.,* 181(7-8), 1288-1312 (2026). https://doi.org/10.1080/10420150.2025.2592201

Sarani, M., Haghighi, H., Tamaddon, P., Darroudi, M., Safari, A., Dastgheib, S. A. and Sattarahmady, N., Bi_2O_3@folic acid nanoparticles: An effective sonosensitizer for melanoma sonodynamic therapy, *Environ. Technol. Innov.*, 41, 104741 (2026). https://doi.org/10.1016/j.eti.2025.104741

Somasundaram, S., Jayabalakrishnan, D., Balajikrishnabharathi, A. and Bhaskar, K., Performance evaluation of silane-treated Cissus quadrangularis fiber and waste Limonia acidissima hull powder on mechanical, fatigue, and water absorption properties of epoxy resin composite, *Biomass Convers. Biorefin.*, 14(5), 6205–6213 (2024). https://doi.org/10.1007/s13399-022-03602-x

Loganathan, T. G., Kumar, V. K., Balasubramanian, M., Gopalan, V., Hasan, S. B. A. and Balaji, K. A., Ensuring the potential of Caryota urens fruit stem fibre as biodegradable reinforcement for polymer composite structural applications, *Biomass Convers. Biorefin.*, 15(8), 12915–12930 (2025). https://doi.org/10.1007/s13399-024-06111-1

Tochaikul, G., Tanadchangsaeng, N., Panaksri, A. and Moonkum, N., Enhancing Radiation Shielding Capabilities with Epoxy-Resin Composites Reinforced with Coral-Derived Calcium Carbonate Fillers, *Polym.*, 17(1), 113 (2025). https://doi.org/10.3390/polym17010113

Unagar, V., May, N., Makwana, R., Barala, S. S. and Purohit, A., Radiation shielding performance of natural rubber composites: A Monte Carlo and XCOM-based study, *Appl. Radiat. Isot.*, 233, 112628 (2026). https://doi.org/10.1016/j.apradiso.2026.112628

Urooge, S., Irshad, A., Jamil, U., Fazil, S., Liaqat, K., Shahzad, K., Alam, F. and Alam, M., Enhanced Gamma Radiation Shielding Using Epoxy Quartz Fabric Composites Reinforced with $CoCl_2$ Microparticles, *Adv. Eng. Mater.*, 28(8), 202502506 (2026). https://doi.org/10.1002/adem.202502506

Venkatesan, S. P., Boobalan, L., Bennet, S., Hemanandh, J. and Ganesan, S., Mechanical properties and morphological study on palm Fiber/S-Glass reinforced polymer matrix composites, *Mater. Today: Proc.*, 47, 4373–4377 (2021). https://doi.org/10.1016/j.matpr.2021.05.184

Xiao, M., Qin, Q., He, X., Li, F. and Wang, X., Shielding Capability Research on Composite Base Materials in Hybrid Neutron-Gamma Mixed Radiation Fields, *Mater.*, 16(5), 2084 (2023). https://doi.org/10.3390/ma16052084

Yuvaraj, G., Myilsamy, S., Sakravathy, N. V. and Kumar, D. R., Effect of Vinyl Silane Treated Bast Fibers and Wood Biomass Filler Incorporated Epoxy Resin Composite – A Characterization Study, *Silicon*, 18(5), 1649–1661 (2026). https://doi.org/10.1007/s12633-025-03589-w